

HUMAN GENETICS

Genomic signatures of the unjamming transition in compressed human bronchial epithelial cells

Margherita De Marzio^{1,2,*†}, Ayşe Kılıç^{1†}, Enrico Maiorino¹, Jennifer A. Mitchel², Chimwemwe Mwase², Michael J. O'Sullivan², Maureen McGill², Robert Chase¹, Jeffrey J. Fredberg², Jin-Ah Park², Kimberly Glass^{1,3‡}, Scott T. Weiss^{1,2,*‡}

Epithelial tissue can transition from a jammed, solid-like, quiescent phase to an unjammed, fluid-like, migratory phase, but the underlying molecular events of the unjamming transition (UJT) remain largely unexplored. Using primary human bronchial epithelial cells (HBECs) and one well-defined trigger of the UJT, compression mimicking the mechanical effects of bronchoconstriction, here, we combine RNA sequencing data with protein-protein interaction networks to provide the first genome-wide analysis of the UJT. Our results show that compression induces an early transcriptional activation of the membrane and actomyosin network and a delayed activation of the extracellular matrix (ECM) and cell-matrix networks. This response is associated with a signaling cascade that promotes actin polymerization and cellular motility through the coordinated interplay of downstream pathways including ERK, JNK, integrin signaling, and energy metabolism. Moreover, in nonasthmatic versus asthmatic HBECs, common genomic patterns associated with ECM remodeling suggest a molecular connection between airway remodeling, bronchoconstriction, and the UJT.

INTRODUCTION

While performing its routine barrier and immune functions, the cellular collective that defines a confluent epithelial tissue is typically quiescent, solid-like, and nonmigratory. In a variety of circumstances, however, the epithelial collective undergoes an unjamming transition (UJT) to become dynamic, fluid-like, and migratory (1–14). For example, experimental data from both in vitro (1–3, 5, 7, 11, 15) and in vivo (2, 6) studies have shown that a UJT occurs spontaneously during physiological events such as embryonic development (2, 6, 9) and during pathophysiological events including wound repair (1, 16) and cancer metastasis (4, 8, 9, 17, 18). In addition, certain stimuli associated with lung pathology such as ionizing radiation (IR) (19) and mechanical compression (2, 11, 15) can also trigger the UJT. In the jammed phase, each cell becomes virtually frozen in place, trapped by its immediate neighbors, in a collective phase where intercellular rearrangements are rare. Conversely, in the unjammed phase, intercellular rearrangements are frequent and the confluent cellular collective moves cooperatively, collectively, and vigorously in packs and swirls reminiscent of turbulent fluid flow (1, 20, 21).

Experimental studies to date have emphasized functional, morphological, and, to a limited extent, molecular features that define the UJT (2, 9, 11, 17) and that distinguish it from the canonical epithelial-to-mesenchymal transition (EMT) (15). After the EMT, for example, cell-cell junctions become degraded, barrier function becomes compromised, apico-basal polarity is lost, and mesenchymal markers appear. After the UJT, by contrast, none of these events occur (15). Rather, cell shapes become more elongated and more variable, and these morphological changes coincide with increased

motility and cellular cooperativity (11, 15). Hence, during the UJT, the cell layer becomes migratory while retaining its full epithelial character.

Recent insights have begun to elucidate the molecular events underlying the UJT. In a breast cancer model system, for example, *RAB5A* triggers unjamming by promoting internalization of the epidermal growth factor receptor (EGFR), leading to hyperactivation of the extracellular signal-regulated kinase 1/2 (ERK1/2) and phosphorylation of the actin nucleator *WAVE2* (17). In well-differentiated primary human bronchial epithelial cells (HBECs), mechanical compression unjams the epithelial layer (11, 15); activates signaling pathways including EGFR (22–24), transforming growth factor- β (TGF- β) receptor (25, 26), ERK (15, 24), and procoagulant factors (27); and induces an asthma-like transcriptional pattern that involves inflammatory, fibrotic, and remodeling processes (28).

These results establish the UJT as a complex multifactorial program. In doing so, they also emphasize the importance of performing a comprehensive molecular assessment of the UJT, but such an assessment is difficult to achieve with single-gene-targeted approaches. The development of RNA sequencing (RNA-seq) technologies (29) now offers an opportunity to profile the genome-wide transcriptomic signature of the UJT. RNA-seq measures the total cellular content of RNA at the transcript-level, providing information on the key genes activated in a specific condition. This information can be further expanded by integrating molecular interaction data (30), which can be used to infer the functional and causal relationships behind a genomic pattern (30).

Here, we report the first comprehensive genomic profiling of epithelial unjamming. We do so by performing RNA-seq of well-differentiated HBECs after compression, which is known to mimic the mechanical effects of bronchospasm and to trigger the UJT (10, 11, 15, 22, 26, 31, 32). We analyze the transcriptional patterns of compressed HBECs at three time points (baseline, 3 hours after compression, and 24 hours after compression) and integrate the RNA-seq data with protein-protein interaction (PPI) networks to identify the molecular pathways represented in these patterns. Our analysis shows that compression-induced UJT in HBECs is not the

Copyright © 2021
The Authors, some
rights reserved;
exclusive licensee
American Association
for the Advancement
of Science. No claim to
original U.S. Government
Works. Distributed
under a Creative
Commons Attribution
NonCommercial
License 4.0 (CC BY-NC).

¹Channing Division of Network Medicine, Department of Medicine, Brigham and Women's Hospital and Harvard Medical School, Boston, MA, USA. ²Department of Environmental Health, Harvard TH Chan School of Public Health, Boston, MA, USA. ³Department of Biostatistics, Harvard TH Chan School of Public Health, Boston, MA, USA. *Corresponding author. Email: scott.weiss@channing.harvard.edu (S.T.W.); nhmdm@channing.harvard.edu (M.D.M.)

†These authors contributed equally to this work as co-first authors.

‡These authors contributed equally to this work as co-last authors.

result of a single biological process but rather the result of the coordinated interplay of multiple downstream pathways involving actin repolymerization, ERK and c-Jun N-terminal kinase (JNK) signaling, and extracellular matrix (ECM) reorganization.

RESULTS

Compression-induced UJT activates three transcriptional regimes

To investigate the biological mechanisms driving the UJT, we harvested HBECs, grew them to confluence under air-liquid interface (ALI), and then exposed them to an apico-to-basal compressive pressure difference of 30-cm H₂O (15, 27, 28, 33) (see Materials and Methods). Following the same experimental protocol described in Kılıç *et al.* (28), this pressure was maintained for 3 hours and then released (Fig. 1A). We assessed the gene expression profile of compressed HBECs using bulk RNA-seq at two time points: immediately after pressure release (3-hour time point) and when cells had rested for an additional 21 hours after pressure removal (24-hour time point). For both time points, RNA-seq was also performed on noncompressed control HBECs.

We selected this experimental protocol for three reasons. First, the magnitude and duration of compression applied to HBECs mimic that experienced by the airway epithelium during asthmatic bronchoconstriction (22, 31, 32). Second, the exposure of HBECs to this mechanical stress has been linked to pathologic responses such as asthmatic airway remodeling (32). Last, this level of compression triggers a distinct UJT that has been thoroughly characterized biophysically and morphologically through a combination of immunofluorescence imaging, live imaging, and computational analysis (11, 15), as described below.

Recent studies (11, 15) have investigated the morphological features of postcompression HBECs under the same experimental conditions as our system. In the absence of compression, control HBECs are arrayed in a disordered cobblestone pattern and are essentially frozen in place, exhibiting only rare and small local rearrangements as in a solid-like, jammed phase. Beginning at 8 hours after compression, cells become more elongated and more variable in shape (11, 15) and the epithelial layer becomes more fluid-like, displaying swirling and collective patterns of migratory behavior (11, 15). At 24 hours after compression, HBECs show all the cardinal features of an unjammed epithelium (11, 15, 34), followed by progressively increasing migration and elongation up to 72 hours after compression (15). These structural and dynamic changes have been explained in terms of a compression-induced UJT arising from increased cellular propulsion and cooperativity (11, 15).

In addition to these structural and dynamic changes, our RNA-seq data showed that compression activated a complex transcriptional response. We assessed this response by performing differential expression analysis of postcompression HBECs at 3 and 24 hours with respect to control samples at the same time points.

At the 3-hour time point, differential expression analysis identified 283 differentially expressed (DE) genes [fold change (FC) > 1.5 and false discovery rate (FDR)-adjusted $P < 0.05$]; this included 89 down-regulated and 194 up-regulated genes (table S1). At the 24-hour time point, we observed 42 genes underexpressed and 171 genes overexpressed (table S2).

DE genes at 3 hours versus 24 hours revealed notable differences in their postcompression transcriptional responses. To characterize

these differences, we computed the z scores of the normalized expression values and performed hierarchical clustering on the DE genes identified at each time point (see Materials and Methods). On the basis of the clustering results, we focused on groups of DE genes that exhibited three characteristic transcriptional responses: transient, long term, and increasing.

A substantial portion of the DE genes at 3 hours (233 of 283, 82%) returned to their baseline expression level at 24 hours (Fig. 1B and table S3, A and B). As a quantitative confirmation of this observation, we calculated the Pearson correlation coefficient of the FC values between 3 hours versus control and 24 hours versus 3 hours ($\rho = -0.84$). These transcriptional changes suggest the activation of a transient regime that reflects the immediate, but temporary, response of cells to mechanical stimulus.

For 109 of the 213 DE genes at 24 hours (table S4), transcriptional activity was unchanged at 3 hours but increased only at 24 hours (Fig. 1B). We note that these genes were identified as DE at 24 hours after compression with respect to both the 3- and 24-hour control samples, excluding the possibility that this behavior is due to changes over time in control gene expression. These results indicate that mechanical stimulus causes a delayed effect on HBEC gene expression and activates a specific, long-term transcriptional program. This transcriptionally active program at 24 hours corresponds to the beginning of a large and sustained increase in cellular unjamming, which continues to at least 72 hours (15).

Last, 42 genes (table S5), which included both overlapping genes and DE genes at 24 hours, exhibited a persistent increase in their expression levels (Fig. 1B). This reflects the activation of an increasing transcriptional regime where the alterations generated by compression increase at each time point.

Overall, the compression triggered a response where transient effects at 3 hours were accompanied by both increasing and delayed effects over time. To identify the signaling pathways associated to these transcriptional patterns, we performed a pathway overrepresentation test on cellular component (CC) and biological process Gene Ontology (GO) annotations (35) using the R package Cluster Profiler (36); results were selected on the basis of an FDR-adjusted P value threshold of 0.05 (see Materials and Methods).

Enrichment analysis using CC annotations revealed that, at 3 hours, DE gene products were localized mainly in the cell membrane and cytoplasm (Fig. 1C), with actin cytoskeleton (FDR = 1.6×10^{-9}) and cell leading edge (FDR = 6.3×10^{-5}) among the most enriched components. At 24 hours, the effects of the mechanical stress shifted from the cellular surface to the endoplasmic reticulum and the ECM space, exhibiting high enrichment in the endoplasmic reticulum lumen (FDR = 2.1×10^{-8}), complex of collagen trimers (FDR = 1.4×10^{-8}), and basement membrane (FDR = 5.5×10^{-6}).

In addition, the transient, increasing, and long-term regimes segregated into different GO BPs, highlighting distinct functions for each gene subset. We identified the major categories enriched in each response by visualizing enriched pathways through a network representation (Fig. 2). Transiently down-regulated genes at 3 hours were exclusively annotated to developmental and differentiation pathways (Fig. 2A and table S6A). The temporary suppression of cell fate decision and cell cycle functions in response to stress has been observed in several studies (37), and this behavior is directly related to the capacity of cells to adapt to environmental conditions.

Conversely, transiently overexpressed genes at 3 hours were mapped to five main BP (Fig. 2A and table S6B): actomyosin structure

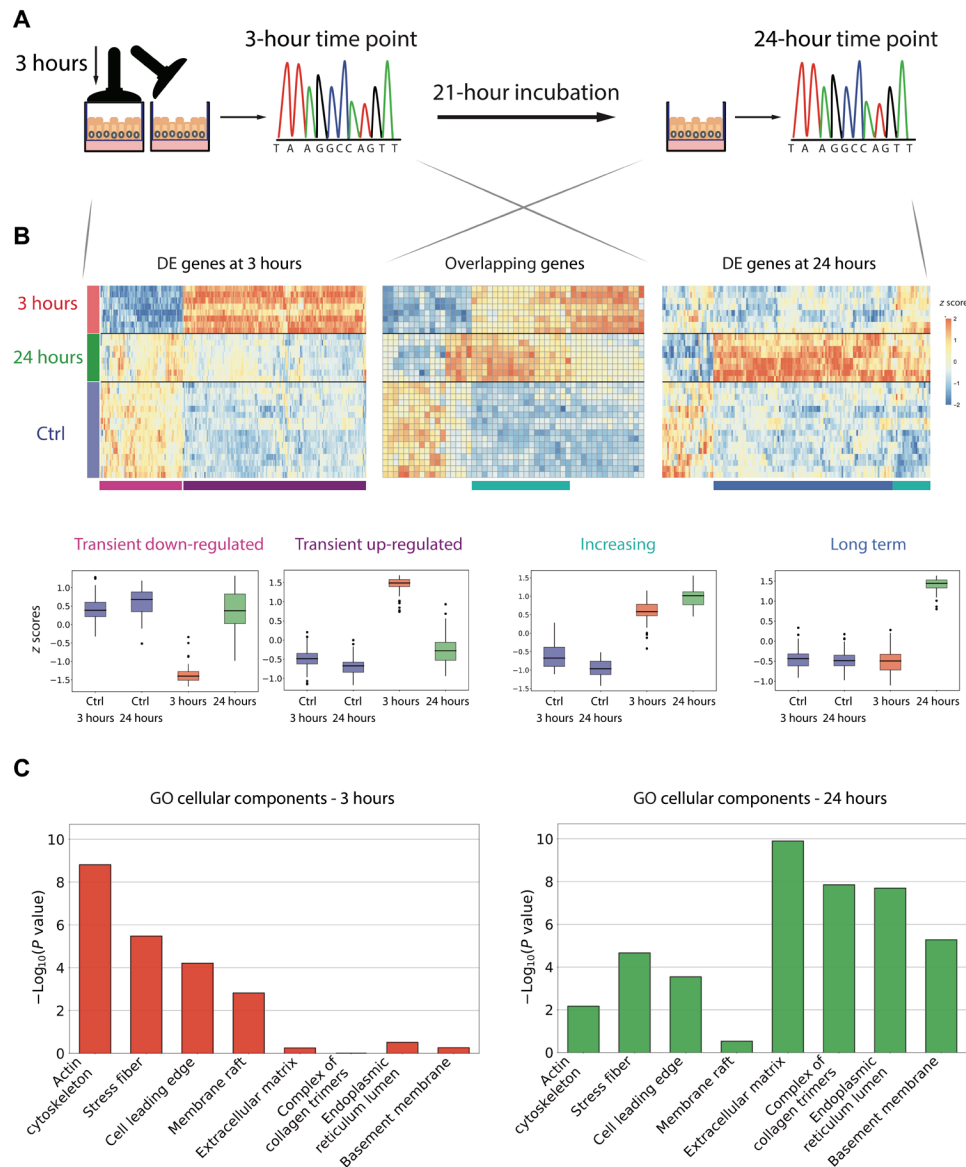


Fig. 1. Overall scheme of the transcriptional patterns activated by compression. (A) The experimental setup: Mechanical compression was applied to well-differentiated HBECs for 3 hours and subsequently released. RNA-seq was extracted from postcompression HBECs immediately after pressure release (3-hour time point) and after an additional 21 hours (24-hour time point). (B) Top: Heatmaps of the normalized expression values at each time point [control (ctrl), 3, and 24 hours] for DE genes at 3 hours (left), DE genes at both 3 and 24 hours (center), and DE genes at 24 hours (right). Rows are z score–normalized for visualization purposes. (B) Bottom: Boxplots of the genes' z scores in the three transcriptional regimes identified by clustering the data shown on top. Each transcriptional regime is noted at the bottom of the heatmap through a specific color: transient down-regulated (pink), transient up-regulated (purple), increasing (teal), and long term (blue). (C) $\log(P \text{ value})$ of a merged subset of Gene Ontology cellular components (GO CC) enriched at 3 and 24 hours. At 3 hours (left), terms associated with the cytoskeleton and cellular membrane are highly enriched compared to the terms associated with the extracellular space. At 24 hours (right), this trend is inverted, and GO terms related to collagen complexes and ECM become highly overrepresented.

organization (FDR = 1.7×10^{-4}), tissue migration (FDR = 8.1×10^{-4}), ERK1/2 cascade (FDR = 4.4×10^{-4}), regulation of mitogen-activated protein kinase (MAPK) activity (FDR = 3.7×10^{-3}), and wound healing (FDR = 3.7×10^{-3}).

DE genes annotated to cytoskeleton reorganization included the actin genes *ACTA1* and *CTG1* and actin-binding and regulating genes such as *CDC42EP2*, *RHOB*, *FHDC1*, *LCPI*, *PLS3*, and *RASSF1*. In addition, genes annotated to cell migration included the soluble factors *HBEGF*, *F3*, and *SRF*, as well as genes involved in actin and myosin regulation such as *HMOX1*, *EGR3*, *MYH9*, and *MYADM*.

These proteins are known to induce collective movement by promoting actin repolymerization and formation of focal adhesion complexes (38). The enrichment analysis also highlighted multiple genes involved in the ERK cascade signaling, such as sprouty proteins *SPRED1*, *SPRED2*, and *SPRY2* and the focal adhesion kinase (FAK) subfamily gene *PTK2B*.

Pathways associated with wound healing included angiogenesis, blood coagulation, and platelet aggregation. These pathways are active during development and repair processes and require reorganization of the cytoskeleton along the leading edge of the cell to facilitate either tissue growth or wound closure (39).

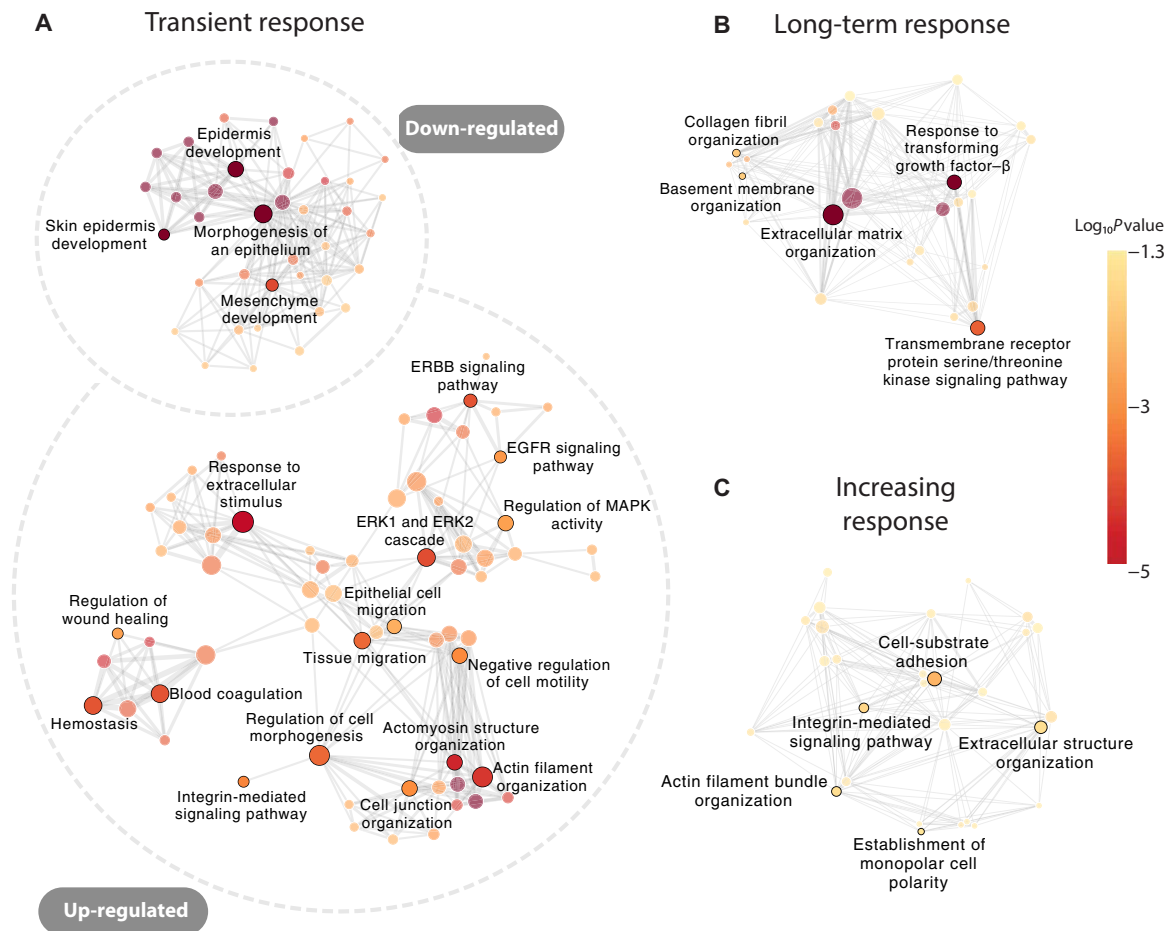


Fig. 2. Pathways enriched in the three transcriptional regimes triggered by compression. For each transcriptional regime, we visualized enriched GO BP using a network representation where each node represents a pathway, and edges between pairs of nodes represent common DE genes annotated to both pathways. For visualization purposes, we showed only edges with more than three common DE genes. Node size and color are based on the number of DE genes annotated to the pathway and its adjusted P value, respectively. (A) GO BP enriched in the transient response, (B) GO BP enriched in the long-term response, and (C) GO BP enriched in the increasing response.

While DE genes at 3 hours were mainly annotated to biological processes regulating the actomyosin network, genes involved in the long-term transcriptional response were mainly annotated to TGF- β receptor and ECM signaling processes (Fig. 2B and table S6C). Extracellular structure organization and collagen fibril organization were enriched in matrix metalloproteinases such as *MMP2* and *MMP10* and in multiple collagen α chain genes, including collagens type I, III, IV, and V. Overexpression of these genes points to a possible reorganization of the ECM at 24 hours, a key process to maintain cell movement by allowing flexible attachment of cells to the substratum (39). GO terms associated with TGF receptor were annotated to target genes of TGF- β 1 signaling such as *NOX4*, *THBS1*, and *PMEPA1*.

Last, enrichment analysis of the increasing genes revealed annotations to molecular processes involving cell-substrate adhesion, actin filament bundle organization, and extracellular structure organization (Fig. 2C and table S6D). Among these genes, TGF- β 1-induced transcript 1, *TGFB1I1*, as well as actin-binding genes *FLNA*, *CNN1*, and *MYL9* showed fold increases larger than two at both the 3- and 24-hour time points. Increased coexpression of these proteins has been

recently connected to the formation of Rho-associated kinase (ROCK)-dependent actin fibers downstream of *TGFB1I1* induction, suggesting a potential role of this gene in regulating cell migration (40).

Our analysis highlights a transcriptional reprogramming of the active regulators of cell shape and motility at the 3-hour time point and of the active regulators of cell-substratum interactions at the 24-hour time point. In a confluent monolayer of Madin-Darby canine kidney-II (MDCKII) cells, it has been recently shown that the structural and dynamical changes of cells undergoing the UJT are accompanied by increased glycolytic activity and larger mitochondrial membrane potential (41). This work led us to investigate the potential role of metabolic processes in our model system. We found that GO terms enriched at 3 hours included the regulation of lipid metabolic process (FDR = 7×10^{-3}), the regulation of small-molecule metabolic process (FDR = 8.5×10^{-3}), and the regulation of cellular carbohydrate metabolic process (FDR = 2.8×10^{-2}). These processes involve oxidation of fatty acids that are subsequently metabolized in mitochondria to produce adenosine triphosphate (ATP) (42). Genes annotated to the enriched pathways included known gluco-regulators and transporters such as *SNCA*, *SESN2*, and *SLC7A11*

(table S7) (43–45). The mitochondrial carrier protein *SLC25A25* was also highly up-regulated at 3 hours (FC = 4.9), suggesting increased mitochondrial activity in support of ATP production (45). Notably, we did not observe any enrichment in metabolic processes at 24 hours. These results hint at a potential mechanism linking UJT with energy metabolism.

Integrins, ERK, and JNK signaling pathways drive the epithelial cell response to compression

Different transcriptional patterns observed at 3 and 24 hours after compression raise the question of which signaling pathways underlie this genomic response in the 21 hours following pressure release. To identify these processes, we first determined which pathways of the Kyoto Encyclopedia of Genes and Genome (KEGG) (46) database were enriched in a merged set of DE genes at 3 and 24 hours (see Materials and Methods). We set the FC threshold of the differential expression analysis to 1.2 and the FDR-adjusted *P* value threshold to 0.05, which resulted in a total of 1512 DE genes across the two time points.

Among the 29 statistically significant KEGG pathways (fig. S1), focal adhesion and MAPK signaling were the most enriched (FDR-adjusted $P = 4.74 \times 10^{-5}$ and 9.95×10^{-5} , respectively). Similar pathways also emerged using the Reactome database (47) (table S8). Given the predominant role of focal adhesions in cytoskeleton reorganization and cell migration, we analyzed the DE genes associated with the focal adhesion pathway at each time point in greater detail (table S9A). At the membrane localization, compression altered the expression of several alpha and beta integrin subunits (Fig. 3A). While *ITGB3* and *ITGB6* were overexpressed at both time points, other integrin chains were selectively induced either at 3 hours (*ITGA2* and *ITGA5*) or at 24 hours (*ITGA4*, *ITGB5*, and *ITGAV*).

In addition to these transmembrane receptors, we found up-regulation of the small guanosine triphosphatase protein encoded by *RAP1B* (3 hours) and of multiple actin-binding adaptor genes such as *VCL* (3 hours), *ZYX* (3 and 24 hours), *SRC* (24 hours), and *FLNA* (24 hours); these genes are known to transmit mechanical forces between the ECM and the actin cytoskeleton (48). Multiple collagen chains were overexpressed only at 24 hours, while the ECM

gene tenascin C (*TNC*) was highly overexpressed at both time points. These findings highlight the recruitment of several integrin-ECM adhesive complexes, suggesting a possible reorganization of the actomyosin network and of the ECM downstream to the integrin signaling (48). Western blots of Tenascin C secreted into the basolateral conditioned media collected from HBECs at 24 hours after pressure confirmed a significant increase of this protein's levels, supporting a potential remodeling of the microenvironment due to exposure of HBECs to compression (fig. S2).

The MAPK signaling pathway was also highly enriched (table S9B). Multiple components involved in the ERK1/2 pathways were strongly overexpressed (Fig. 3B), including genes encoding growth factors; Ras-family proteins *RAP1B* (3 hours), *RASA2* (3 hours), and *mRAS* (24 hours); and the transcription factors *FOS* (3 and 24 hours), *ATF4* (3 hours), and *SRF* (3 hours). Compression also activated several molecules related to the JNK signaling pathway, such as *MAP3K1* (3 hours) and *MAP3K8* (3 hours), and the proto-oncogenes *JUND* (3 hours) and *JUN* (3 and 24 hours). These results, combined with the overexpression of genes in the dual-specificity phosphatase (DUSP) family at 3 and 24 hours, which are known counterregulators of MAPK (49), hint at a differential fine-tuning of MAPK signaling.

In contrast to the consistent overexpression of integrins, other growth factors and receptors—such as *FGFR3* (3 and 24 hours), *ANGPT1* (24 hours), and *PDGFA/D* (3 and 24 hours, respectively)—were down-regulated. Similarly, the expression of the cytosolic phospholipases *PLA2G4D*, *PLA2G4E*, and *PLA2G4F* was reduced at 24 hours.

To extract additional information on the active signaling cascade involving these focal adhesion and MAPK components, we combined our RNA-seq data with known protein interactions contained in PPI databases. PPIs can be represented as a network made up of proteins (nodes) that are linked to each other based on physical binding interactions (edges) (30). The PPI network represents a powerful tool to infer information on the cell signaling pathways occurring in a specific process. In particular, analysis of network paths, defined by the sequences of edges that connect two nodes, can be used to identify the molecular processes that transmit signal between two proteins.

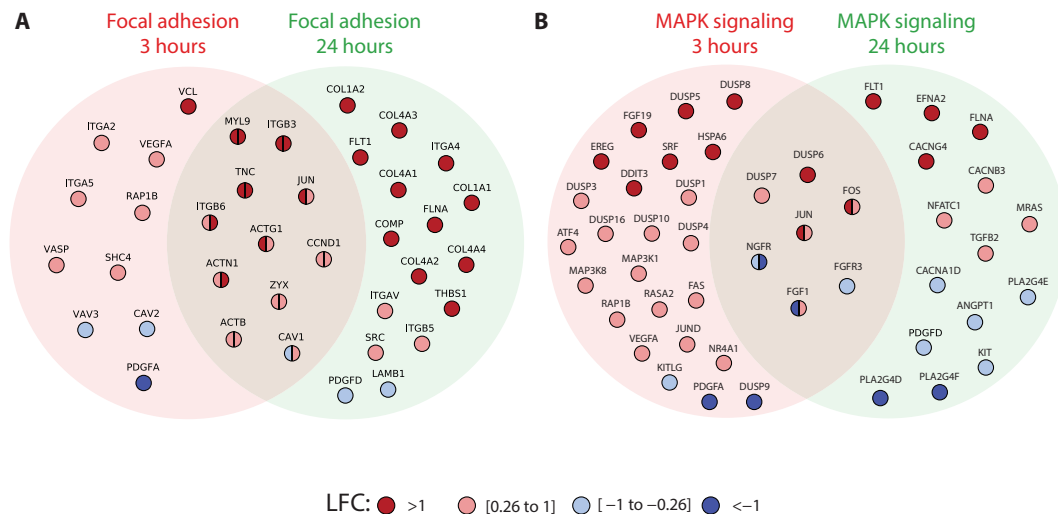


Fig. 3. DE genes annotated to the KEGG focal adhesion and MAPK signaling pathways. Overview of DE genes at 3 and 24 hours, color-coded on the basis of their log FC (LFC), which are also annotated to the (A) focal adhesion or (B) MAPK signaling pathways.

Following a procedure similar to the one proposed in (50), we modeled a signal transduction process as a sequential path on the network that starts from a receptor, connects the receptor to multiple kinases, and leads to a transcription factor (TF) (Fig. 4A). This receptor-kinase-transcription factor (RKT) path representation mimics the typical pattern of signaling cascades, where the signaling transmission is triggered by membrane-bound receptors, propagates via intracellular kinases, and ultimately regulates the activity of TFs (51).

We used the databases developed in (52) and (53) for the selection of receptors and kinases, respectively. To focus our analysis on the RKT paths that have a major impact on the long-term transcriptional response, we selected TFs that specifically target DE genes at 24 hours (see Materials and Methods).

Starting from a recently proposed PPI (54) (see Materials and Methods), we filtered the network to derive two subgraphs that contained the receptors/kinases annotated to the focal adhesion and

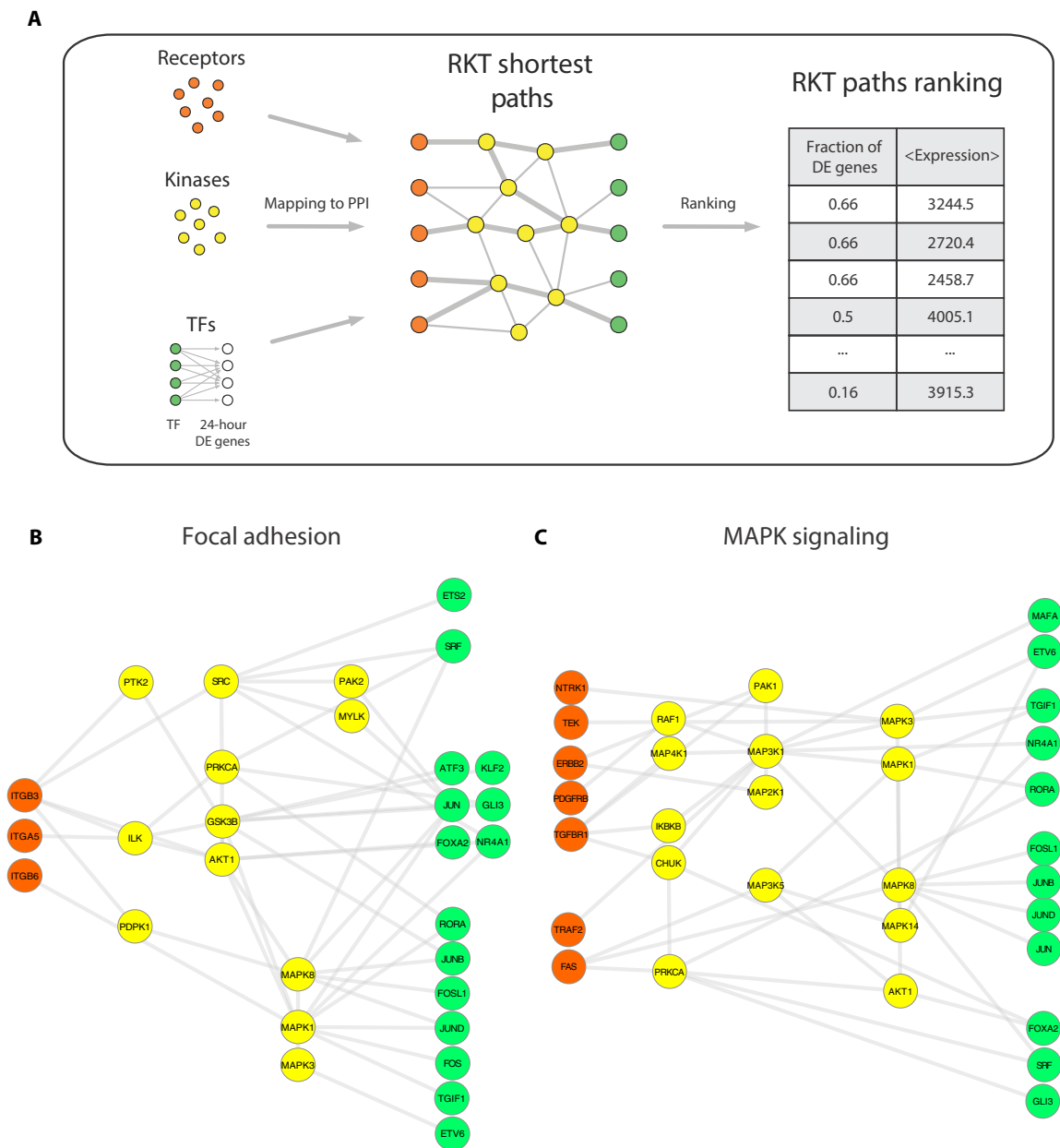


Fig. 4. RKT analysis. (A) Overview of the network analysis used to identify the RKT paths. First, the PPI network is filtered for receptors, kinases, and transcription factors (TFs) that affect DE genes at 24 hours. Within this subnetwork, we identified all the shortest paths (RKT paths) starting from a receptor, connecting up to five layers of kinases, and ending in a transcription factor. RKT paths were ranked on the basis of the fraction of their nodes that are DE at 3 hours and on the average expression of their nodes at 3 hours. (B) Top-ranked RKT paths containing nodes annotated to the focal adhesion pathway. (C) Top-ranked RKT paths containing nodes annotated to the MAPK signaling pathway. Note that PPI edges do not have directionality, and, hence, the placement of the nodes in (B) and (C) has been chosen on the basis of biological considerations associated with the RKT paths.

MAPK signaling pathway, respectively, as well as the set of TFs described above. We assumed a one-to-one correspondence between genes and their protein products in the entire analysis. For each signaling subgraph, we computed all the shortest paths connecting each receptor TF pair (see Materials and Methods). We then ranked these RKT paths based on the fraction of DE genes in each path and used the average expression of the path's nodes at 3 hours to break the ties (Fig. 4A). The top selected paths represent the most active downstream processes induced by compression [for a detailed list of all the network paths identified, see table S10 (A and B)].

The top RKT paths within the focal adhesion subgraph were initiated by integrins ITGA and ITGB (Fig. 4B), showing a predominant role of these ECM receptors compared to receptor tyrosine kinases. The integrin-induced paths emphasized three main downstream signaling directions: (i) the engagement of *SRC* and *MYLK* kinases, both implicated in actin contractility (55); (ii) the activation of activator protein 1 (AP-1) transcription factors such as *JUN*, *JUNB*, and *ATF3* via the ILK-AKT1/GSK3B signaling path, known to regulate AP-1 activity through phosphorylation of *AKT1* and *GSK3B* by the kinase *ILK* (56); and (iii) the activation of multiple *FOS* and *JUN* homodimers via *MAPK1* and *MAPK8*, highlighting the role of ERK2 and JNK signaling in the transmission of the mechanical stimulus.

A detailed view of the MAPK signaling RKT paths (Fig. 4C) revealed the engagement of various growth factor receptors—including *NTRK1*, *TGFBR1*, *TEK*, and *ERBB2*—and cytokine receptors (*FAS*). In agreement with the results in the focal adhesion subnetwork, the active RKT paths in the MAPK subgraph suggested the downstream regulation of the ERK1/2 pathway via the cascade *MAP3K1*, *MAPK1*, and *MAPK3* and of the JNK pathway via *MAPK8*. In addition, the overrepresentation of RKT paths including *PRKCA*, *CHUK*, *IKBKB* and the nuclear receptors *NR4A1* and *RORA* highlighted the participation of the nuclear factor κ B pathway in the signal transmission.

The focal adhesion and MAPK RKT paths pointed to the downstream engagement of 16 TFs. To determine the main processes regulated by these TFs, we performed a pathway overrepresentation test using the 24-hour DE genes that are targeted by these 16 TFs (see Materials and Methods). Top GO BP (table S11 and fig. S3) included extracellular structure organization (FDR = 1.3×10^{-8}), response to TGF- β (FDR = 2.6×10^{-8}), and positive regulation of cell migration (FDR = 2.6×10^{-6}). Notably, we found a large overrepresentation of metabolic processes involving the biosynthesis of cholesterol and alcohol, supporting the activation of specific metabolic programs during the UJT.

The RKT analysis predicted signaling pathways that are consistent with the morphological changes observed during the UJT. Reorganization of the actomyosin network and activation of AP-1 transcription factors are both essential mechanisms to regulate cellular shape and motility. Since these processes involve multiple components that are not only receptors, kinases, or TFs, we further investigated our network analysis considering the entire PPI.

Flow centrality predicts key genes mediating the transcriptional response of HBECs to compression

We expanded our network analysis to determine, at a genome-wide level, which genes have a major role in mediating the molecular processes triggered by compression. To achieve this goal, we considered

a recently proposed “betweenness” centrality measure called flow centrality (57).

In network theory, the betweenness centrality of a node is defined as its frequency among all the shortest paths that traverse a network. Flow centrality extends this definition, encompassing only the shortest paths connecting any node in a specific source subset to any node in a specific target subset. The flow central score (FCS) quantifies the significance of the flow centrality of each node by comparing its value to a null distribution obtained by randomizing source and target node sets (see Materials and Methods). In the PPI network, genes with high FCS, called “flow central genes,” are more likely to be involved in the interactions connecting source and target gene sets of interest, constituting a topological bottleneck in the communication between the two subsets.

In our study, we chose the DE genes at 3 and 24 hours as source and target sets, respectively, and applied flow centrality to select the genes involved in the interactions between these two gene sets. A total of 556 flow central genes with FCS > 2 were identified (see Material and Methods and table S12).

To determine potential functional similarities among the flow central genes, we clustered them based on their shared source and target genes and investigated the network properties of each of the resulting clusters (see Materials and Methods). For each flow central cluster, we calculated a “connectivity score” $f_{S/T}^c$. This quantity is defined as the average fraction of flow central genes connected to at least one source or target gene (see Materials and Methods). High values of $f_{S/T}^c$ imply high connectivity of the flow central cluster with respect to the source/target set.

Our clustering analysis identified five main clusters (Fig. 5A and table S13). Except for one cluster that had low connectivity with both source and target gene sets, the identified four clusters exhibited markedly different connectivity features with respect to the source and target genes. Cluster 1 and cluster 4 were highly connected to the source and target set, respectively (Fig. 5B). In contrast, cluster 2 and cluster 3 exhibited $f_{S/T}^c > 0.5$ both for the source and target genes.

The connectivity score is proportional to the number of shortest paths connecting a cluster to the source/target and, hence, indirectly provides information on the functional affinity of the clusters to the DE genes at the two time points. Since the DE genes at 3 hours were mainly associated with membrane proteins, and DE genes at 24 hours were mainly associated with ECM and collagen proteins, the decreasing source connectivity and increasing target connectivity from clusters 1 to 4 suggested a gradual propagation of the signal from the membrane to the cellular nucleus, transmitted via the flow central clusters. To test this hypothesis, we looked at the relative abundance of each cluster in three main GO CC: the membrane (GO: 0016020), the cytosol (GO: 0005829), and the nucleus (GO: 0005634). The fraction of genes localized in the membrane decreased from clusters 1 to 4 as source connectivity decreases, while proteins localized in the cytosol and nucleus increased (Fig. 5C). This suggests that the flow central genes in cluster 1 represent the first mediators of the signal, while the remaining clusters represent the gradual signal transduction to the proteins responsible for the late transcriptional response observed at 24 hours.

The identified flow central genes were consistent with the signaling pathways highlighted in the previous section. To show this, we compared the FCS distribution of the genes annotated to focal adhesion and MAPK signaling pathways to the FCS distribution of the remaining genes in the PPI. For both pathways, the FCS of

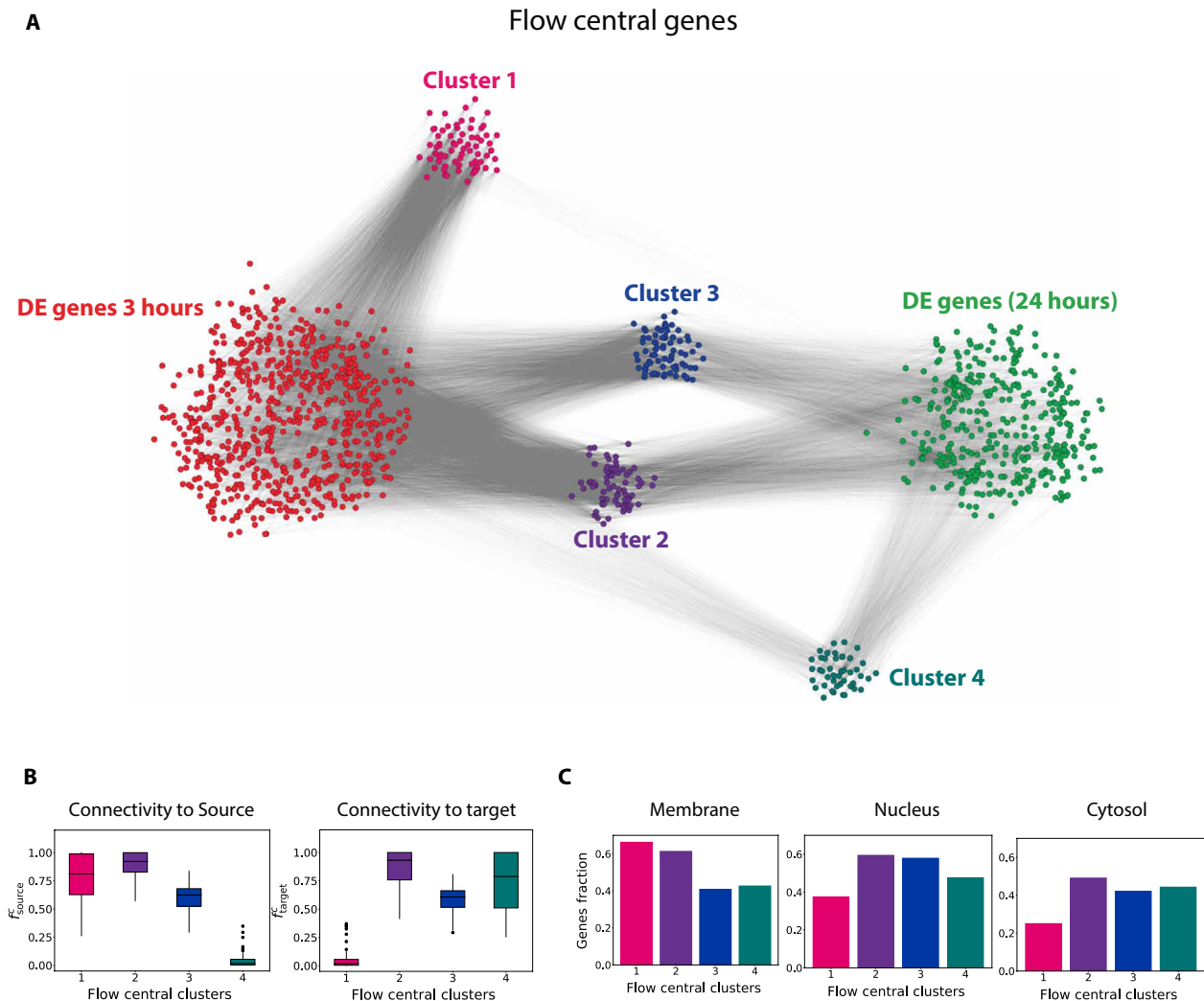


Fig. 5. Flow centrality analysis. (A) Network visualization of the flow central clusters identified using flow centrality. Edges between each pair of source/target-flow central nodes indicate that the two nodes are connected via a network shortest path. For visualization purposes, we showed only a random 10% of total number of edges. (B) Connectivity score of each flow central cluster with respect to the source (left) and the target (right) gene sets. (C) Relative fraction of genes in each cluster that are annotated to the membrane, nucleus, and cytosol GO terms.

annotated genes was statistically higher (Mann-Whitney U test, $P = 1.3 \times 10^{-15}$ for focal adhesion and $P = 6 \times 10^{-9}$ for MAPK signaling) than the FCS of other genes (fig. S4). It follows that flow centrality supports a leading role of focal adhesion molecules and MAPKs in the communication between the two transcriptional responses at 3 and 24 hours.

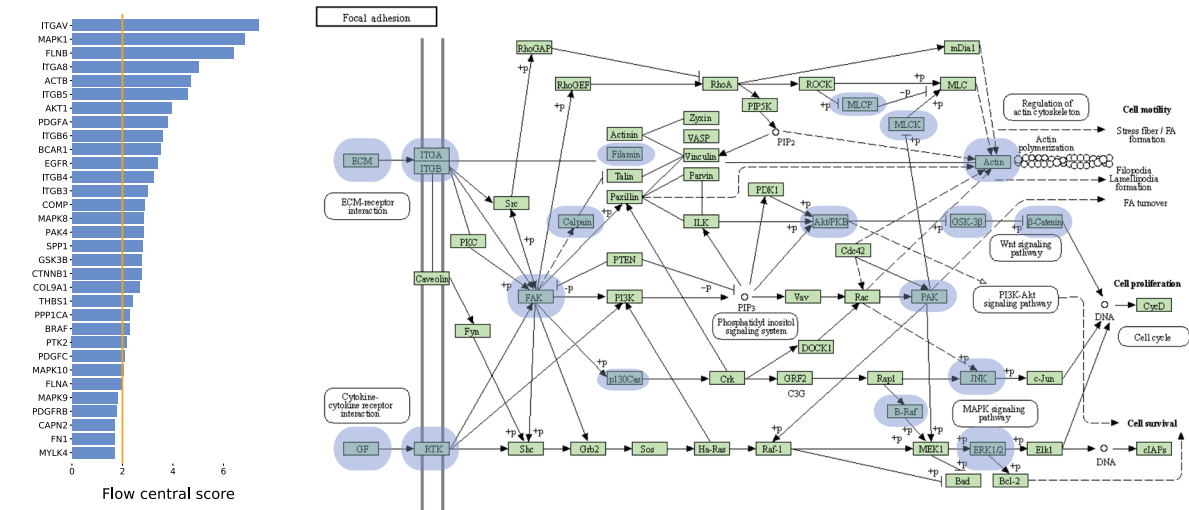
Flow central genes included multiple genes identified in the RKT analysis. Flow central genes annotated to either the focal adhesion or MAPK signaling pathway overlapped significantly (hypergeometric $P < 1 \times 10^{-3}$) with genes in the RKT paths—including *PTK2*, *AKT1*, *MAPK1*, and *MAPK8*—as well as additional components, thus confirming and extending by an independent methodology the network predictions obtained through the RKT path analysis.

Several integrins showed high FCS, including *ITGAV*, *ITGB3*, *ITGB4*, *ITGB5*, and *ITGB6* (Fig. 6A). These molecules bind to ECM proteins with their extracellular head region and to the actin cytoskeleton via intracellular proteins that attach to their cytoplasmic

domain (58). In agreement with this mechanism, both matrix proteins *SPP1* and *FN1* and adapter proteins *FLNB* and *FLNA* displayed high FCS (Fig. 6A). Additional flow central genes included *PTK2*, *PAK4*, and *CAPN2*, central bottlenecks for the regulation of actin polymerization and for the propagation of downstream signaling pathways within the cell (59).

Among these pathways, we found high FCS of the JNK-associated components *MAP2K7*, *MAPK8/9/10*, *MAPK8IP1*, and *JUND* and of the ERK2-associated proteins *BRAF* and *MAPK1*. Notably, *MAPK1* showed a high FCS of 6.83 (Fig. 6B), implying a potential pivotal role of this gene in driving collective migration during the UJT. The overrepresentation of genes involved in the ERK and JNK signaling pathways corroborated the crucial contribution of these processes to mechanical stimulus transduction in HBECs. In addition, the high FCS of *AKT1*, *GSK3B*, and *CTNBN1*, known to modulate cellular apoptosis via regulation of β -catenin activity (Fig. 6A) (60), provided a possible explanation for the inhibition of cell proliferation previously observed in our system (11, 15).

A Focal adhesion flow central genes



B MAPK signaling flow central genes

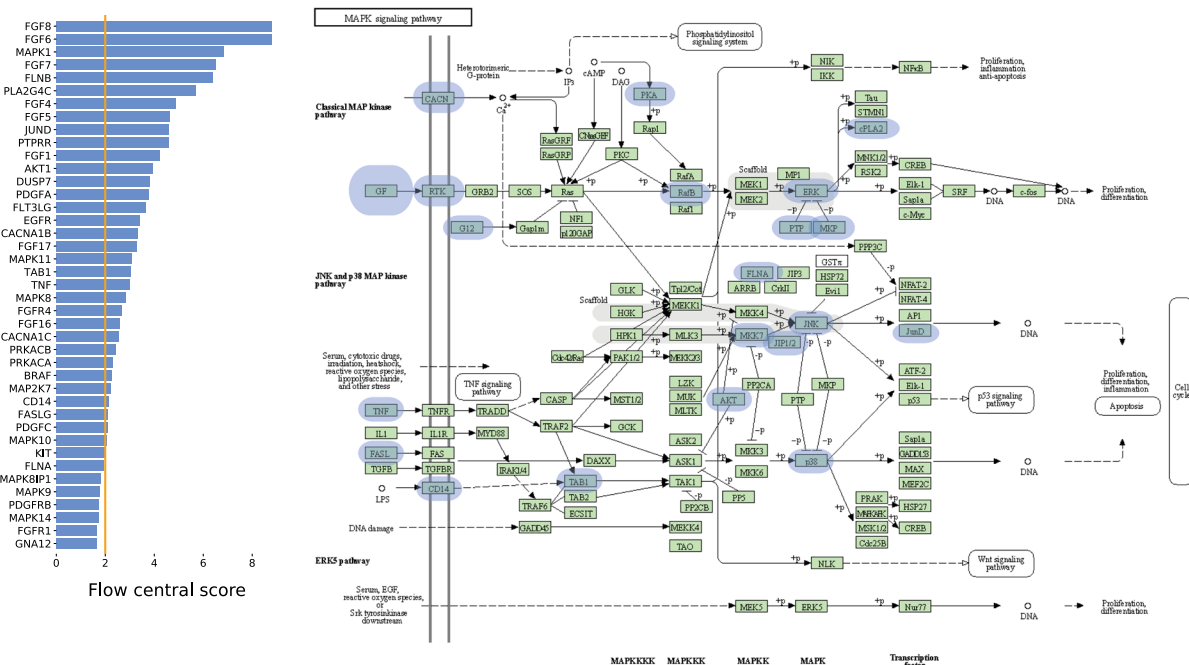


Fig. 6. Role of the flow central genes in the focal adhesion and MAPK signaling pathway. Flow central score of genes associated with the (A) focal adhesion and (B) MAPK signaling pathways. For each pathway, the FCSs of the top flow central genes are shown in the left panel. In the right panel, the location of each of the flow central genes within the KEGG (46) pathway representation is highlighted.

We also observed a high FCS for multiple fibroblast growth factors and their corresponding receptors. This result may imply a parallel activation of the ERK pathway via signal transmission to adaptor proteins such as *GRB2*, *SOS*, and *Ras* (61).

Overall, this analysis showed that the morphological and migratory changes that are hallmarks of the UJT are accompanied at the molecular level by transcriptional activation of genes involved in actin repolymerization, JNK- and ERK-mediated regulation of cell motility, and β -catenin reorganization. This suggests that cells undergoing the UJT trigger a specific transcriptional program that

allows remodeling of the cytoskeleton network and of the adhesive interactions with the ECM.

Flow centrality identifies ECM remodeling proteins as key regulators of the structural changes induced by compression of asthmatic HBECs

Park *et al.* (11) showed that unjamming not only is relevant in the context of mechanotransduction but also has implications for aberrant airway remodeling, a cardinal feature of asthma. Compared with HBECs derived from nonasthmatic donors, HBECs derived from

asthmatic donors exhibit phenotypic characteristics of unjammed tissues, with more elongated shapes and prominent collective migratory behavior (11). At the transcriptional level, a recent study has shown that asthmatic HBECs and nonasthmatic HBECs at 24 hours after compression exhibit similar transcriptional patterns as genes associated with airway remodeling and ECM reorganization (28).

Similarities between asthmatic HBECs at baseline and nonasthmatic HBECs postcompression can be traced back to the effect of asthmatic bronchoconstriction on the airway. During bronchoconstriction, airway smooth muscle contracts, this contraction narrows the airway, and this airway narrowing compresses the airway epithelial layer (22, 31, 32). Even in the absence of inflammatory stimuli, this compression is sufficient to recapitulate key anatomic and pathophysiologic changes observed during asthmatic bronchoconstriction (26, 32). Therefore, we investigated the potential existence of common molecular components involved in the unjamming of both asthmatic and compressed normal epithelial cells. To achieve this task, we assessed the transcriptional profile of ALI-cultured HBECs from four asthmatic donors through bulk RNA-seq. RNA-seq data were extracted at baseline, consistent with the experimental setup of compressed normal HBECs (see Materials and Methods). We performed differential expression analysis on the asthmatic HBECs versus the control (unperturbed HBECs at baseline) using the R package DESeq2. By choosing a threshold of FC > 1.5 and FDR-adjusted $P < 0.05$, we identified 253 DE genes (see Materials and Methods and table S14).

We compared DE genes in nonasthmatic HBECs at 24 hours after compression to DE genes in asthmatic HBECs at baseline (no pressure) using the same FC threshold (FC > 1.5). The two sets significantly overlapped (hypergeometric $P = 4.6 \times 10^{-12}$), and the sign of the FC of the DE genes at 24 hours after compression and in asthmatic HBECs was positively correlated (correlation coefficient $\rho = 0.4$, $P = 1.8 \times 10^{-9}$) (see Materials and Methods and fig. S5). Next, we applied flow centrality. We selected the DE genes at 3 hours after compression in normal HBECs as the source gene set, and we considered two different sets of genes as targets: (i) the DE genes at 24 hours after compression in normal HBECs and (ii) the DE genes in asthmatic cells without any perturbation. To remove potential similarities due to the same source genes, the FCS was computed by randomizing only the target module (see Materials and Methods). The two resulting sets of FCS, displayed in Fig. 7, represented the specificity of each gene in the PPI in connecting the source to the target modules as compared to a random set of target genes.

While multiple genes showed different values of FCS between the two datasets, a statistically significant subset of 57 flow central genes (table S15) appeared to mediate both the transcriptional response of nonasthmatic HBECs at 24 hours after compression and asthmatic HBECs at baseline. Many of these common flow central genes are implicated in the regulation of ECM, cell-matrix interactions, and cell-cell adhesive junctions. High values of FCS were assigned to both ECM proteins such as *COL16A1*, *FN1*, *MATN2*, and *FBLN2* and to focal adhesion proteins such as *ITGAV* and *FLNB*. Common flow central genes also included *MAPKBP1*, *MAPK1*, and *JUND*, highlighting the potential role of JNK and ERK signaling cascades in both phenomena. In both asthmatic and compressed normal HBECs, flow centrality identified molecules such as *VEZT*, a component of the cadherin-catenin complex critical to the formation of adherens junctions (62), and the metalloproteinases *ADAM12* and *MMP9*, proteins known to be involved in the degradation of

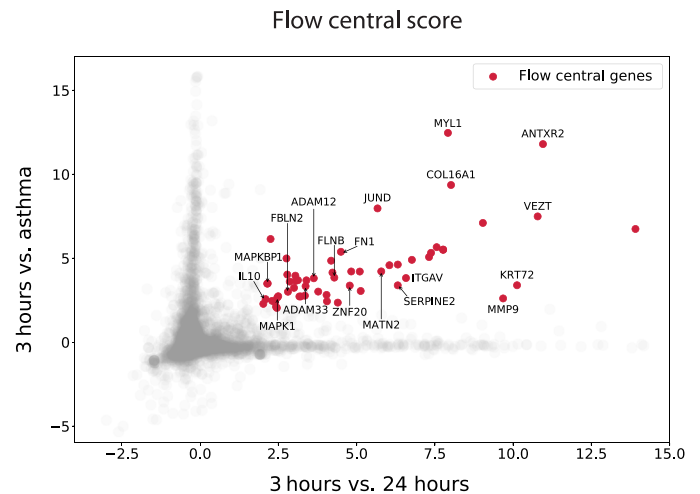


Fig. 7. Flow centrality in asthma. The FCS of each PPI node was calculated by applying flow centrality to DE genes at 3 hours versus DE genes at 24 hours (x axis), as well as DE genes at 3 hours versus genes DE in asthma (y axis). Common flow central genes (FCS > 2 in both analyses) are highlighted in red.

the ECM (63), as key mediators of the signal transmission. Not only are the common flow central genes involved in the structural reorganization of the intercellular and ECM-interactions, but also they have been shown to be associated with the airway remodeling processes observed in asthmatic airways as a consequence of bronchoconstriction (26).

DISCUSSION

This analysis shows that the HBEC transcriptional response to compression is characterized by transient and long-term effects involving different molecular regulators of the mechanical properties of the epithelium. Immediately after pressure release (3-hour time point), HBECs transcriptionally reprogram cytoskeletal genes regulating the structure of the actomyosin network; at 21 hours after pressure release (24-hour time point), HBECs activate a delayed transcriptional response involving the ECM and its interaction with the cellular basal membrane. By using a network-based approach, we show that these genomic patterns are associated with multiple, coordinated signaling pathways that induce cell shape changes via actin repolymerization processes and increased cell motility via ERK- and JNK-mediated activation of AP-1 transcription factors. This analysis points to possible links at the genomic level between HBECs compression, the UJT, and airway remodeling (31).

These RNA-seq data and network analyses highlight a central role of integrins. Integrins are heterodimeric proteins consisting of α and β chains that can be combined to give rise to 24 unique integrin molecules (58). By binding to cytoskeletal and matrix proteins, these transmembrane receptors serve both as signaling centers and as loci for exertion of the traction forces that propel cell migration (58). Force transmission mechanisms mediated by integrins have been extensively described (14, 64). Nevertheless, limited knowledge has been achieved on the systematic relationship between these receptors and cellular motion. Our study revealed that integrins were DE up to 24 hours after pressure exposure and were involved in multiple signaling pathways, suggesting a role of these heterodimers

as more than simple mechanoreceptors. This result, together with the delayed overexpression of several ECM genes, hints at the potential activation of a positive feedback between the epithelial genetic response and the mechanical properties of the substratum, where cell-ECM adhesion components are steadily recruited by integrins to assist and stabilize cellular unjamming.

In agreement with this scenario, our analysis shows that these receptors are involved in both actin polymerization processes via SRC and the focal adhesion kinase PTK2, as well as additional downstream signals activating the transcription factors JUN and FOS via ERK1/2 and JNK pathways. Although these pathways are known to be triggered in response to mechanical stress (24), the picture that emerges from our study indicates that ERK1/2 and JNK are active regulators of cell motility as early as several hours after the initial application of pressure. Notably, both these signaling pathways have been previously associated with the collective migration of cells in epithelial sheets (15, 65, 66). We recently showed (15) that, after blocking ERK activity using the pharmacological inhibitor U0126, compressed HBECs exhibit significantly reduced motility and cooperativity with an average cellular speed that is comparable to uncompressed HBECs. Propagation of ERK1/2 waves has been also observed to be correlated with collective cell movements in a wound healing assay of MDCK cells (65). In addition, the JNK pathway has been connected to the regulation of collective migration of several cell types in wound healing and developmental processes (66).

Mechanotransduction processes do not necessarily require the differential expression of their involved genes and can be activated as early as seconds after an external stimulus (67). It follows that the signaling pathways identified by our study likely represent the molecular processes sustaining the UJT, leaving room for speculation on what is the initial trigger that induces this phenomenon. Previous studies performed by us and by others have shown that mechanical compression on HBECs stimulates downstream ERK signaling by activating EGFR and its ligands only 20 min after pressure application, suggesting the possible preexistence of latent forms of these growth factors in the epithelial tissue (22). In addition, our RNA-seq data are compatible with the possible activation of cell receptors via conformational changes or physical aggregation of these molecules, irrespective of their specific ligand. For example, compression and stretch can directly induce structural changes in integrins (68), growth factor receptors (69), and ion channels (70). These alterations have been reported together with rapid activation of downstream intracellular pathways, including phosphoinositide 3-kinase, ERK, and JNK signaling (68–70). Given the pronounced transcriptional response we observed at the 3-hour time point, it is conceivable that similar events occur in vivo in compressed airway epithelial cells during asthmatic bronchospasm.

Limitations of this study include a small sample size. The integration of additional types of -omics data and a larger sample size would allow us to further investigate undetected molecular processes, such as epigenetic and posttranslational modifications. A larger number of subjects would also allow us to compare with asthmatic cells, given the heterogeneity of this disease. Another limitation is the RNA isolation process, which prevents the epithelial tissue from being sequenced and analyzed through live imaging at the same time and in the same sample. We have had to rely on separate experiments under the same conditions to make the inferences described here.

A variety of mechanical and nonmechanical stimuli are now known to promote the UJT in HBECs including compression (15),

asthma (11), and IR (19). Hence, our current study raises the question of whether we are identifying the broad molecular response of HBECs to compression versus the subset of events that specifically underlie the UJT. To investigate this, we used IR in the context of a candidate gene approach and performed real-time quantitative polymerase chain reaction (RT-qPCR) on four candidate genes that were highlighted in both our differential expression and network analysis: ACTB, FLNA, DUSP7, and NEDD9. ACTB and FLNA are known regulators of integrin-induced actin repolymerization (58), DUSP7 is a known regulator of ERK and JNK pathways (49), and NEDD9 is a known regulator of cellular motility both via integrin-induced focal adhesion stabilization and via JNK pathways (71). Our results support a potential role of DUSP7 and NEDD9 in mediating radiation-induced unjamming, but not ACTB or FLNA (fig. S6). The universality of the UJT across stimuli remains to be comprehensively investigated, and our analysis of transcriptomics and molecular interactions in the case of compression of HBECs is only the first step toward better characterizing the UJT at the genome-wide level. Nevertheless, these findings establish that compression-induced responses of HBECs involve the coordinated interplay of downstream pathways, including development, energy metabolism, and cytoskeletal and ECM reorganization, consistent with the morphological and dynamical changes observed during the UJT.

By highlighting the value of a system biology approach in studying the UJT, our study motivates the investigation of novel biological hypotheses and suggests new experimental directions. On the one hand, the design of targeted experiments will be crucial for elucidating the functional mechanisms and causative impact of the candidate genes identified in our work. On the other hand, our results raise questions about the universality of the UJT transcriptional program across different physiological and pathophysiological contexts. Future bulk and single-cell RNA-seq experiments, as well as spatially resolved transcriptomic experiments, will be critical for answering these important questions.

MATERIALS AND METHODS

Experimental design

Primary HBECs and mechanical compression

Primary HBECs were derived from four donors with no preexisting chronic lung disease and four asthmatic donors following the same protocol as described previously (11). HBECs were grown for 5 to 6 days to reach confluency and subsequently cultured in ALI conditions (11). For each donor, two independent replicates were introduced into the polarization process.

On ALI day 14, well-differentiated nonasthmatic HBECs were exposed to 30-cm H₂O apical-to-basal mechanical compression for 3 hours as described in (11), and after this time, pressure was released. Compressed nonasthmatic HBECs were harvested both immediately after pressure release, referred in the text as the 3-hour time point, and after a further incubation period of 21 hours, referred in the text as the 24-hour time point. Control and asthmatic noncompressed HBECs were also harvested at the same reference time points. Harvested cells were used for isolation of RNA.

RNA isolation, library preparation, and RNA-seq

Total RNA was isolated organically using QIAzol lysis reagent and the QIAGEN miRNeasy Kit (QIAGEN). Quality was assessed using the NanoDrop 8000 spectrophotometer. Sequencing libraries were constructed with the TruSeq Stranded Total RNA Library Prep Globin

Kit (Illumina). Sequencing was performed using a HiSeq 2500 instrument (Illumina). Raw reads were trimmed with Skewer (72) and then mapped to the GRCh38 reference genome using STAR (73). Read counts were computed with HTSeq (74). Data were normalized using DESeq2 (75).

Statistical analysis

Differential expression analysis

Differential expression analysis was performed using the R package DESeq2 (v.1.22.2) (75). Three separate DE analyses were performed: nonasthmatic compressed HBECs at 3 hours versus nonasthmatic uncompressed HBECs at 3 hours, nonasthmatic compressed HBECs at 24 hours versus nonasthmatic uncompressed HBECs at 24 hours, and asthmatic versus nonasthmatic uncompressed HBECs. Genes with zero counts across all the different conditions were removed. For the first two DE analyses, the design matrix was built to take into account batch effects in cells derived from the same donor. In the third DE analysis between uncompressed asthmatic versus nonasthmatic HBECs, both the 3- and 24-hour time points were included, and thus, the design matrix was implemented to remove temporal batch effects. In all the DE analyses, we applied DESeq2-independent filtering, and *P* values were corrected for multiple hypothesis testing by using the Benjamini-Hochberg (BH)-FDR adjustment.

Hierarchical clustering to identify the three transcriptional regimes

The three transcriptional regimes (transient, long term, and increasing) described in the main text were identified by performing hierarchical clustering on the *z* scores of the normalized expression counts. Specifically, raw counts were normalized and transformed for variance stabilization using the DESeq2 function VST (variance stabilizing transformation). We then performed a hierarchical clustering on the counts' *z* scores using the Euclidean distance and the complete-linkage metrics. We cut the cluster dendrogram so that we obtained two clusters for DE genes only at 3 hours, six clusters for DE genes only at 24 hours, and four clusters for DE genes at both 3 and 24 hours. On the basis of the clustering results, we selected three specific clusters corresponding to three characteristic transcriptional responses: transient, long term, and increasing.

Enrichment analysis: GO, KEGG, and Reactome enrichment analysis

For each transcriptional regime, we performed GO overrepresentation tests using the "enrichGO" function in the R package "clusterProfiler" (v.3.10.1) (36), setting as a background the gene set used for the differential expression analysis. In both GO CC and BP terms, we used the R annotation package "org.Hs.eg.db" (v.3.7.0). To identify the most active pathways mediating the different transcriptional regimes, we used the clusterProfiler function "enrichKEGG" to perform KEGG pathway enrichment on the merged set of DE genes at 3 and 24 hours. We confirmed the results of the KEGG enrichment using the Reactome database (47). We performed enrichment analysis on the merged set of DE genes at 3 and 24 hours using the clusterProfiler function "enrichPathway." For all enrichment analyses, *P* values were adjusted using the BH-FDR correction, and an FDR < 0.05 was used to identify significantly enriched pathways.

PPI network

The PPI network used in our network analysis was compiled by Cheng *et al.* (54). As described in the original paper, this PPI network integrates 15 different databases and includes (i) binary PPIs identified via high-throughput yeast-two-hybrid (Y2H) experiments; (ii)

kinase-substrate interactions from literature-derived low-throughput and high-throughput experiments; (iii) literature-curated PPIs identified through affinity purification mass spectrometry (AP-MS), Y2H, literature-derived low-throughput experiments, and protein three-dimensional structures; and (iv) signaling network interactions from literature-derived low-throughput experiments, as annotated in SignaLink2.0. Only the largest connected component of the network was considered, resulting in an interactome of 16,656 proteins and 243,592 interactions.

RKT analysis

As an initial input for the implementation of the RKT analysis, we filtered the PPI network based on a list of receptors (R), kinases (K), and TFs, which were identified as follows. Receptors and kinases were assembled from the curated databases developed in (52) and (53), respectively. For the TFs, we first generated a list of TF motif mappings. To do this, we used FIMO (find individual motif occurrences) (76) to scan the human genome (hg38) for a comprehensive set of CIS-BP (catalog of inferred sequence binding preferences) Single-Species DNA motifs curated in the MEME (multiple em for motif elicitation) suite (77). Hits that met a significance less than 1×10^{-4} and fell within $[-750, +250]$ base pairs of a gene's transcriptional start site [based on gene annotations downloaded from UCSC; (78)] were used to construct a set of TF-gene interactions. We used this mapping to select TFs targeting DE genes at 24 hours after compression. In particular, for each TF, we used the hypergeometric test to compute the *P* value of the overlap between the TF's target genes and DE genes at 24 hours. TFs with a *P* value lower than 0.05 were included in the network. The total selected set of receptors, kinases, and TFs included 1827 genes.

After filtering the PPI network based on this list (1759 nodes), we removed all the R-R, R-TF, K-R, TF-R, TF-K, and TF-TF edges to restrict our analysis to the shortest paths following the RKT directionality. We further filtered the network to only include R and K annotated specifically to either the KEGG focal adhesion (hsa04510) or MAPK (hsa04010) pathways, obtaining two separate subgraphs for each pathway. For each subgraph, we computed all the shortest paths containing one layer of receptor, up to five layers of kinases, and one layer of TFs. Paths that included interactions between different receptor classes were removed, as these interactions typically occur via indirect cross-talk of downstream signaling pathways and do not represent direct ligand-receptor interactions.

To determine the main processes regulated by the most active RKT paths, we selected the genes that were targeted by TFs in each RKT path (based on the TF mapping described above) and that were DE at the 24-hour time point. We performed pathway overrepresentation test on the GO BP enriched in this gene set using clusterProfiler (see above), and we focused on the top 30 enriched pathways (BH-FDR < 0.05). We used all of the genes (DE and not-DE) targeted by the TFs in the RKT paths as a background for the overrepresentation test.

Flow centrality and flow connectivity score

Flow centrality is a topological measure proposed by Maiorino *et al.* (57). The flow centrality $FC^{S,T}(i)$ of a node *i* with respect to a given source *S* and target *T* set of nodes is given by

$$FC^{S,T}(i) = \frac{1}{|S| |T|} \sum_{s \in S, t \in T} \frac{\sigma_{st}(i)}{\sigma_{st}}$$

where $\sigma_{st}(i)$ is the number of shortest paths connecting a source node *s* to a target node *t* passing through node *i*, σ_{st} is the total number

of shortest paths connecting s and t , and $|S|$ and $|T|$ denote the size of the source and target sets, respectively. Given this definition, the FCS of a node represents the statistical significance of a node's flow centrality value with respect to a null distribution of random pairs of source and target gene sets. Specifically, the FCS of a node i is equal to

$$\text{FCS}^{S,T}(i) = \frac{\text{FC}^{S,T}(i) - \mu_{\text{FC}}}{\sigma_{\text{FC}}}$$

where μ_{FC} and σ_{FC} are the average and SD across the distribution of the node's $\text{FC}^{S,T}(i)$ values obtained by computing its flow centrality with respect to 1000 random source and target gene sets [see (57) for details]. High values of FCS indicate that the node occurs more frequently in connecting the source and target modules. Genes with FCS greater than 2 in the PPI are defined as "flow central genes." In contrast to the raw values of flow centrality, the flow central score is not biased toward high-degree nodes.

To determine potential similarities among the 556 flow central genes identified in our analysis, we performed a clustering analysis. For each flow central gene, we created a binary vector representing all source and target nodes; we assigned a value of 1 to an element of this vector if the corresponding source/target node occurred in one of the shortest paths mediated by the flow central gene. We performed an unweighted average linkage clustering on these 556 binary vectors using the Hamming distance metric and identified five main clusters. We then investigated the connectivity properties of each cluster by defining a connectivity score, $f_{S/T}^c$, as

$$f_{S/T}^c = \sum_{i=0}^{N_{S/T}} N_{\text{flow}}^i / S_c$$

where N_{flow}^i is the number of flow central genes in cluster c that connect to source/target node i , S_c is the size of the flow central cluster c , and $N_{S/T}$ is the size of the source and target modules, respectively. The connectivity score measures the relative amount a cluster mediates the communication with the source/target sets.

Comparison between flow central genes in asthmatic HBECs at baseline and in nonasthmatic HBECs at 24 hours after compression

We first compared the transcriptional profiles of (i) nonasthmatic HBECs at 24 hours after compression and (ii) noncompressed asthmatic HBECs by computing the overlap in the DE genes in each condition. We found 14 overlapping genes between DE genes at 24 hours after compression and DE genes in asthmatic cells (hypergeometric $P = 4.64 \times 10^{-12}$). To further identify global patterns of similarities, we selected the DE genes at 24 hours after compression ($\text{FC} > 1.5$ and $\text{BH-FDR} < 0.05$) and compared the sign of their FC value between the two DE analyses. The signs of the FC values were positively correlated, with a Pearson correlation coefficient of $\rho = 0.4$ and two-tailed $P = 1.8 \times 10^{-9}$, showing similar perturbations in the genomic patterns of nonasthmatic postcompression cells and asthmatic cells.

For the comparison between the flow central genes connecting nonasthmatic postcompression HBECs at 3 hours versus 24 hours and nonasthmatic postcompression HBECs at 3 hours versus asthmatic HBECs, we modified the original definition of FCS to remove non-informative similarities in the calculation of the flow centrality values due to the same source set. To account for these biases, we randomized only the target module in the computation of the FCS, following the same randomization protocol described in (57). It follows that

the resulting FCS expresses the statistical significance of the flow central values by comparing them with a null distribution where only the target set is variable. This approach allowed us to estimate similarities between flow central genes that are related only to the specific target sets chosen.

Experimental validation

Protein expression analysis

To detect secreted ECM protein Tenascin C in response to compression by Western blot analysis, basolateral conditioned media were collected at 24 hours from HBECs with or without compression. In both conditions, equal amounts of protein were concentrated from the basolateral conditioned media to pellets using 20% trichloroacetic acid. Pellets were washed with ice-cold acetone three times and suspended in 10 μl of 2 \times SDS-polyacrylamide gel electrophoresis (SDS-PAGE) buffer, boiled, and loaded on the 10% SDS-PAGE as described previously (79, 80). Transferrin was detected as a loading control.

Quantitative real-time RT-qPCR

We detected mRNA expression in HBECs exposed to two different stimuli known to induce the UJT: mechanical compression and IR. For the radiation-induced UJT, primary HBECs from two donors with no preexisting chronic lung diseases were ALI-cultured and were exposed to subtherapeutic doses (1 gray) of IR on days 7, 10, and 14 of ALI culture [using the same protocol described in (19)]. Two independent replicates were introduced for each donor. RNA was extracted at 24 hours after the final IR exposure. For the compression-induced UJT, RNA was extracted from compressed HBECs (six donors with no preexisting chronic lung diseases) at 24 hours after the onset of pressure using the same protocol described in Materials and Methods.

RNA was extracted from cells using the RNeasy Mini Kit (QIAGEN, Valencia, CA) according to the manufacturer's instructions. One microgram of total RNA was used to synthesize complementary DNA (cDNA) using MultiScribe reverse transcriptase (Applied Biosystems, Foster City, CA). RT-qPCR was performed using 25 ng of cDNA and 2 \times SYBR Green PCR Mastermix. Primers specific for *ACTB* (5'-GGACTTCGAGCAAGAGATGG-3'/5'-AGGAAGGAAG-GCTGGAAGAG-3'), *DUSP7* (5'-ATCCCCATCTCTGACCCTG-3'/5'-TAGGCGTCGTTGAGTGACAG-3'), *NEDD9* (5'-ATGTCCAC-GTCTTCCACCTC-3'/5'-TTAGGCTGGAGACACCCATC-3'), *FLNA* (5'-GGAGGAGGCAAAAGTGACCG-3'/5'-ACTTATCCAC-GTACACCTCGAAG-3'), and *GAPDH* (5'-TGGGCTACACTGAG-CACCAG-3'/5'-GGGTGTCGCTGTTGAAGTCA-3') were used to test the mRNA expression. PCR quantification was done with the comparative $\Delta\Delta\text{Ct}$ method, with normalization to *GAPDH* as the housekeeping gene.

SUPPLEMENTARY MATERIALS

Supplementary material for this article is available at <http://advances.sciencemag.org/cgi/content/full/7/30/eabf1088/DC1>

[View/request a protocol for this paper from Bio-protocol.](#)

REFERENCES AND NOTES

1. T. E. Angelini, E. Hannezo, X. Trepat, M. Marquez, J. J. Fredberg, D. A. Weitz, Glass-like dynamics of collective cell migration. *Proc. Natl. Acad. Sci. U.S.A.* **108**, 4714–4719 (2011).
2. L. Atia, D. Bi, Y. Sharma, J. A. Mitchel, B. Gweon, S. A. Koehler, S. J. DeCamp, B. Lan, J. H. Kim, R. Hirsch, A. F. Pegoraro, K. H. Lee, J. R. Starr, D. A. Weitz, A. C. Martin, J. A. Park, J. P. Butler, J. J. Fredberg, Geometric constraints during epithelial jamming. *Nat. Phys.* **14**, 613–620 (2018).

3. S. Garcia, E. Hannezo, J. Elgeti, J. F. Joanny, P. Silberzan, N. S. Gov, Physics of active jamming during collective cellular motion in a monolayer. *Proc. Natl. Acad. Sci. U.S.A.* **112**, 15314–15319 (2015).
4. A. Haeger, M. Krause, K. Wolf, P. Friedl, Cell jamming: Collective invasion of mesenchymal tumor cells imposed by tissue confinement. *Biochim. Biophys. Acta* **1840**, 2386–2395 (2014).
5. C. Malinverno, S. Corallino, F. Giavazzi, M. Bergert, Q. Li, M. Leoni, A. Disanza, E. Frittoli, A. Oldani, E. Martini, T. Lendenmann, G. DeFlorian, G. V. Beznoussenko, D. Poulikakos, K. H. Ong, M. Uroz, X. Trepap, D. Parazzoli, P. Maiuri, W. Yu, A. Ferrari, R. Cerbino, G. Scita, Endocytic reawakening of motility in jammed epithelia. *Nat. Mater.* **16**, 587–596 (2017).
6. A. Mongera, P. Rowghanian, H. J. Gustafson, E. Shelton, D. A. Kealhofer, E. K. Carn, F. Serwane, A. A. Lucio, J. Giammona, O. Campàs, A fluid-to-solid jamming transition underlies vertebrate body axis elongation. *Nature* **561**, 401–405 (2018).
7. K. D. Nnetu, M. Knorr, J. Käs, M. Zink, The impact of jamming on boundaries of collectively moving weak-interacting cells. *New J. Phys.* **14**, 115012 (2012).
8. L. Oswald, S. Grosser, D. M. Smith, J. A. Käs, Jamming transitions in cancer. *J. Phys. D Appl. Phys.* **50**, 483001 (2017).
9. J.-A. Park, L. Atia, J. A. Mitchel, J. J. Fredberg, J. P. Butler, Collective migration and cell jamming in asthma, cancer and development. *J. Cell Sci.* **129**, 3375–3383 (2016).
10. J.-A. Park, J. J. Fredberg, Cell jamming in the airway epithelium. *Ann. Am. Thorac. Soc.* **13**, S64–S67 (2016).
11. J.-A. Park, J. H. Kim, D. Bi, J. A. Mitchel, N. T. Qazvini, K. Tantisira, C. Y. Park, M. McGill, S. H. Kim, B. Gweon, J. Notbohm, R. Steward Jr., S. Burger, S. H. Randell, A. T. Kho, D. T. Tambe, C. Hardin, S. A. Shore, E. Israel, D. A. Weitz, D. J. Tschumperlin, E. P. Henske, S. T. Weiss, M. L. Manning, J. P. Butler, J. M. Drazen, J. J. Fredberg, Unjamming and cell shape in the asthmatic airway epithelium. *Nat. Mater.* **14**, 1040–1048 (2015).
12. M. Sadati, N. T. Qazvini, R. Krishnan, C. Y. Park, J. J. Fredberg, Collective migration and cell jamming. *Differentiation* **86**, 121–125 (2013).
13. A. F. Pegoraro, J. J. Fredberg, J.-A. Park, Problems in biology with many scales of length: Cell–cell adhesion and cell jamming in collective cellular migration. *Exp. Cell Res.* **343**, 54–59 (2016).
14. X. Trepap, M. R. Wasserman, T. E. Angelini, E. Millet, D. A. Weitz, J. P. Butler, J. J. Fredberg, Physical forces during collective cell migration. *Nat. Phys.* **5**, 426–430 (2009).
15. J. A. Mitchel, A. Das, M. J. O'Sullivan, I. T. Stancil, S. J. De Camp, S. Koehler, O. H. Ocaña, J. P. Butler, J. J. Fredberg, M. A. Nieto, D. Bi, J.-A. Park, The unjamming transition is distinct from the epithelial-to-mesenchymal transition. *Nat. Commun.* **11**, 5053 (2020).
16. X. Serra-Picamal, V. Conte, R. Vincent, E. Anon, D. T. Tambe, E. Bazellieres, J. P. Butler, J. J. Fredberg, X. Trepap, Mechanical waves during tissue expansion. *Nat. Phys.* **8**, 628–634 (2012).
17. A. Palamidessi, C. Malinverno, E. Frittoli, S. Corallino, E. Barbieri, S. Sigismund, G. V. Beznoussenko, E. Martini, M. Garre, I. Ferrara, C. Tripodo, F. Ascione, E. A. Cavalcanti-Adam, Q. Li, P. P. Di Fiore, D. Parazzoli, F. Giavazzi, R. Cerbino, G. Scita, Unjamming overcomes kinetic and proliferation arrest in terminally differentiated cells and promotes collective motility of carcinoma. *Nat. Mater.* **18**, 1252–1263 (2019).
18. O. Iliina, P. G. Gritsenko, S. Syga, J. Lippoldt, C. A. M. La Porta, O. Chepizhko, S. Grosser, M. Vullings, G.-J. Bakker, J. Starruß, P. Bult, S. Zapperi, J. A. Käs, A. Deutsch, P. Friedl, Cell–cell adhesion and 3D matrix confinement determine jamming transitions in breast cancer invasion. *Nat. Cell Biol.* **22**, 1103–1115 (2020).
19. M. J. O'Sullivan, J. A. Mitchel, A. Das, S. Koehler, H. Levine, D. Bi, Z. D. Nagel, J. A. Park, Irradiation induces epithelial cell unjamming. *Front. Cell Dev. Biol.* **8**, 21 (2020).
20. K. D. Nnetu, M. Knorr, S. Pawlizak, T. Fuhs, J. A. Käs, Slow and anomalous dynamics of an MCF-10A epithelial cell monolayer. *Soft Matter* **9**, 9335–9341 (2013).
21. S.-Z. Lin, W.-Y. Zhang, D. Bi, B. Li, X.-Q. Feng, Energetics of mesoscale cell turbulence in two-dimensional monolayers. *Communications Physics* **4**, 21 (2021).
22. D. J. Tschumperlin, G. Dai, I. V. Maly, T. Kikuchi, L. H. Laiho, A. K. McVittie, K. J. Haley, C. M. Lilly, P. T. C. So, D. A. Lauffenburger, R. D. Kamm, J. M. Drazen, Mechanotransduction through growth-factor shedding into the extracellular space. *Nature* **429**, 83–86 (2004).
23. N. Kojic, E. Chung, A. T. Kho, J. A. Park, A. Huang, P. T. C. So, D. J. Tschumperlin, An EGFR autocrine loop encodes a slow-reacting but dominant mode of mechanotransduction in a polarized epithelium. *FASEB J.* **24**, 1604–1615 (2010).
24. D. J. Tschumperlin, J. D. Shively, M. A. Swartz, E. S. Silverman, K. J. Haley, G. Raab, J. M. Drazen, Bronchial epithelial compression regulates MAP kinase signaling and HB-EGF-like growth factor expression. *Am. J. Physiol. Lung Cell. Mol. Physiol.* **282**, L904–L911 (2002).
25. D. J. Tschumperlin, J. D. Shively, T. Kikuchi, J. M. Drazen, Mechanical stress triggers selective release of fibrotic mediators from bronchial epithelium. *Am. J. Respir. Cell Mol. Biol.* **28**, 142–149 (2003).
26. C. L. Grainge, L. C. K. Lau, J. A. Ward, V. Dulay, G. Lahiff, S. Wilson, S. Holgate, D. E. Davies, P. H. Howarth, Effect of bronchoconstriction on airway remodeling in asthma. *N. Engl. J. Med.* **364**, 2006–2015 (2011).
27. J.-A. Park, A. S. Sharif, D. J. Tschumperlin, L. Lau, R. Limbrey, P. Howarth, J. M. Drazen, Tissue factor–bearing exosome secretion from human mechanically stimulated bronchial epithelial cells in vitro and in vivo. *J. Allergy Clin. Immunol.* **130**, 1375–1383 (2012).
28. A. Kılıç, A. Ameli, J.-A. Park, A. T. Kho, K. Tantisira, M. Santolini, F. Cheng, J. A. Mitchel, M. M. Gill, M. J. O'Sullivan, M. De Marzio, A. Sharma, S. H. Randell, J. M. Drazen, J. J. Fredberg, S. T. Weiss, Mechanical forces induce an asthma gene signature in healthy airway epithelial cells. *Sci. Rep.* **10**, 966 (2020).
29. Z. Wang, M. Gerstein, M. Snyder, RNA-Seq: A revolutionary tool for transcriptomics. *Nat. Rev. Genet.* **10**, 57–63 (2009).
30. M. Vidal, M. E. Cusick, A.-L. Barabási, Interactome networks and human disease. *Cell* **144**, 986–998 (2011).
31. M. J. O'Sullivan, T.-K. N. Phung, J.-A. Park, Bronchoconstriction: A potential missing link in airway remodelling. *Open Biol.* **10**, 200254 (2020).
32. P. C. Veerati, J. A. Mitchel, A. T. Reid, D. A. Knight, N. W. Bartlett, J.-A. Park, C. L. Grainge, Airway mechanical compression: Its role in asthma pathogenesis and progression. *Eur. Respir. Rev.* **29**, 190123 (2020).
33. J. A. Mitchel, S. Antoniak, J.-H. Lee, S.-H. Kim, M. McGill, D. I. Kasahara, S. H. Randell, E. Israel, S. A. Shore, N. Mackman, J.-A. Park, IL-13 Augments Compressive Stress-Induced Tissue Factor Expression in Human Airway Epithelial Cells. *Am. J. Respir. Cell Mol. Biol.* **54**, 524–531 (2016).
34. D. Bi, X. Yang, M. C. Marchetti, M. L. Manning, Motility-driven glass and jamming transitions in biological tissues. *Phys. Rev. X* **6**, 021011 (2016).
35. Gene Ontology Consortium, The Gene Ontology resource: 20 years and still GOing strong. *Nucleic Acids Res.* **47**, D330–D338 (2019).
36. G. Yu, L.-G. Wang, Y. Han, Q.-Y. He, clusterProfiler: An R package for comparing biological themes among gene clusters. *OMICS* **16**, 284–287 (2012).
37. A. Mammoto, D. E. Ingber, Cytoskeletal control of growth and cell fate switching. *Curr. Opin. Cell Biol.* **21**, 864–870 (2009).
38. E. N. Olson, A. Nordheim, Linking actin dynamics and gene transcription to drive cellular motile functions. *Nat. Rev. Mol. Cell Biol.* **11**, 353–365 (2010).
39. G. C. Gurtner, S. Werner, Y. Barrandon, M. T. Longaker, Wound repair and regeneration. *Nature* **453**, 314–321 (2008).
40. D. A. Tumbarello, C. E. Turner, Hic-5 contributes to epithelial-mesenchymal transformation through a RhoA/ROCK-dependent pathway. *J. Cell. Physiol.* **211**, 736–747 (2007).
41. S. J. DeCamp, V. M. K. Tsuda, J. Ferruzzi, S. A. Koehler, J. T. Giblin, D. Roblyer, M. H. Zaman, S. T. Weiss, A. Kılıç, M. de Marzio, C. Y. Park, N. C. Ogassavara, J. A. Mitchel, J. P. Butler, J. J. Fredberg, Epithelial layer unjamming shifts energy metabolism toward glycolysis. *Sci. Rep.* **10**, 18302 (2020).
42. M. Dashty, A quick look at biochemistry: Carbohydrate metabolism. *Clin. Biochem.* **46**, 1339–1352 (2013).
43. J. H. Lee, A. V. Budanov, M. Karin, Sestrins orchestrate cellular metabolism to attenuate aging. *Cell Metab.* **18**, 792–801 (2013).
44. G. Rodriguez-Araujo, H. Nakagami, H. Hayashi, M. Mori, T. Shiuchi, Y. Minokoshi, Y. Nakaoka, Y. Takami, I. Komuro, R. Morishita, Y. Kaneda, Alpha-synuclein elicits glucose uptake and utilization in adipocytes through the Gab1/PI3K/Akt transduction pathway. *Cell. Mol. Life Sci.* **70**, 1123–1133 (2013).
45. Y. Lai, *Transporters in Drug Discovery and Development: Detailed Concepts and Best Practice* (Woodhead Publishing, 2014), chap. 1, pp. 1–146.
46. M. Kanehisa, S. Goto, KEGG: Kyoto encyclopedia of genes and genomes. *Nucleic Acids Res.* **28**, 27–30 (2000).
47. B. Jassal, L. Matthews, G. Viteri, C. Gong, P. Lorente, A. Fabregat, K. Sidropoulos, J. Cook, M. Gillespie, R. Haw, F. Loney, B. May, M. Milacic, K. Rothfels, C. Sevilla, V. Shamovsky, S. Shorsler, T. Vasuraj, J. Weiser, G. Wu, L. Stein, H. Hermjakob, P. D'Eustachio, The reactome pathway knowledgebase. *Nucleic Acids Res.* **48**, D498–D503 (2020).
48. H. B. Schiller, R. Fässler, Mechanosensitivity and compositional dynamics of cell–matrix adhesions. *EMBO Rep.* **14**, 509–519 (2013).
49. C. J. Caunt, S. M. Keyse, Dual-specificity MAP kinase phosphatases (MKPs) shaping the outcome of MAP kinase signalling. *FEBS J.* **280**, 489–504 (2013).
50. M. H. Kabir, R. Patrick, J. W. K. Ho, M. D. O'Connor, Identification of active signaling pathways by integrating gene expression and protein interaction data. *BMC Syst. Biol.* **12**, 77–87 (2018).
51. P. van der Geer, T. Hunter, R. A. Lindberg, Receptor protein-tyrosine kinases and their signal transduction pathways. *Annu. Rev. Cell Biol.* **10**, 251–337 (1994).
52. J. A. Ramilowski, T. Goldberg, J. Harshbarger, E. Kloppmann, M. Lizio, V. P. Satagopam, M. Itoh, H. Kawaji, P. Carninci, B. Rost, A. R. R. Forrest, A draft network of ligand–receptor-mediated multicellular signalling in human. *Nat. Commun.* **6**, 7866 (2015).
53. UniProt - Swiss-Prot Protein Knowledgebase, Human and mouse protein kinases: Classification and index (SIB Swiss Institute of Bioinformatics, Geneva, Switzerland, 2021); www.uniprot.org/docs/pkinfam (accessed 11 December 2019).
54. F. Cheng, R. J. Desai, D. E. Handy, R. Wang, S. Schneeweiss, A.-L. Barabási, J. Loscalzo, Network-based approach to prediction and population-based validation of in silico drug repurposing. *Nat. Commun.* **9**, 2691 (2018).
55. D. J. Webb, K. Donais, L. A. Whitmore, S. M. Thomas, C. E. Turner, J. T. Parsons, A. F. Horwitz, FAK–Src signalling through paxillin, ERK and MLCK regulates adhesion disassembly. *Nat. Cell Biol.* **6**, 154–161 (2004).

56. A. A. Troussard, C. Tan, T. N. Yoganathan, S. Dedhar, Cell-extracellular matrix interactions stimulate the AP-1 transcription factor in an integrin-linked kinase-and glycoprotein synthase kinase 3-dependent manner. *Mol. Cell Biol.* **19**, 7420–7427 (1999).
57. E. Maiorino, S. H. Baek, F. Guo, X. Zhou, P. H. Kothari, E. K. Silverman, A.-L. Barabási, S. T. Weiss, B. A. Raby, A. Sharma, Discovering the genes mediating the interactions between chronic respiratory diseases in the human interactome. *Nat. Commun.* **11**, 811 (2020).
58. J. Z. Kechagia, J. Ivaska, P. Roca-Cusachs, Integrins as biomechanical sensors of the microenvironment. *Nat. Rev. Mol. Cell Biol.* **20**, 457–473 (2019).
59. M. Vicente-Manzanares, A. R. Horwitz, Adhesion dynamics at a glance. *J. Cell Sci.* **124**, 3923–3927 (2011).
60. C.-M. Yang, S. Ji, Y. Li, L.-Y. Fu, T. Jiang, F.-D. Meng, β -Catenin promotes cell proliferation, migration, and invasion but induces apoptosis in renal cell carcinoma. *Oncotargets Ther.* **10**, 711–724 (2017).
61. J. Schlessinger, Common and distinct elements in cellular signaling via EGF and FGF receptors. *Science* **306**, 1506–1507 (2004).
62. P. Küssel-Andermann, A. el-Amraoui, S. Safieddine, S. Nouaille, I. Perfettini, M. Lecuit, P. Cossart, U. Wolfgramm, C. Petit, Vezatin, a novel transmembrane protein, bridges myosin VIIA to the cadherin–catenins complex. *EMBO J.* **19**, 6020–6029 (2000).
63. P. Lu, K. Takai, V. M. Weaver, Z. Werb, Extracellular matrix degradation and remodeling in development and disease. *Cold Spring Harb. Perspect. Biol.* **3**, a005058 (2011).
64. J. H. Kim, X. Serra-Picamal, D. T. Tambe, E. H. Zhou, C. Y. Park, M. Sadati, J. A. Park, R. Krishnan, B. Gweon, E. Millet, J. P. Butler, X. Trepap, J. J. Fredberg, Propulsion and navigation within the advancing monolayer sheet. *Nat. Mater.* **12**, 856–863 (2013).
65. N. Hino, L. Rossetti, A. Marín-Lauradó, K. Aoki, X. Trepap, M. Matsuda, T. Hirashima, ERK-mediated mechanochemical waves direct collective cell polarization. *Dev. Cell* **53**, 646–660.e8 (2020).
66. Y. Xia, M. Karin, The control of cell motility and epithelial morphogenesis by Jun kinases. *Trends Cell Biol.* **14**, 94–101 (2004).
67. J. L. Alonso, W. H. Goldmann, Cellular mechanotransduction. *AIMS Biophys.* **3**, 50–62 (2016).
68. A. Katsumi, T. Naoe, T. Matsushita, K. Kaibuchi, M. A. Schwartz, Integrin activation and matrix binding mediate cellular responses to mechanical stretch. *J. Biol. Chem.* **280**, 16546–16549 (2005).
69. N. Kinoshita, Y. Hashimoto, N. Yasue, M. Suzuki, I. M. Cristea, N. Ueno, Mechanical stress regulates epithelial tissue integrity and stiffness through the FGFR/Erk2 signaling pathway during embryogenesis. *Cell Rep.* **30**, 3875–3888.e3 (2020).
70. S. G. Brohawn, Z. Su, R. MacKinnon, Mechanosensitivity is mediated directly by the lipid membrane in TRAAK and TREK1 K⁺ channels. *Proc. Natl. Acad. Sci.* **111**, 3614–3619 (2014).
71. S. Zhang, L. Wu, Roles of neural precursor cell expressed, developmentally downregulated 9 in tumor-associated cellular processes (Review). *Mol. Med. Rep.* **12**, 6415–6421 (2015).
72. H. Jiang, R. Lei, S.-W. Ding, S. Zhu, Skewer: A fast and accurate adapter trimmer for next-generation sequencing paired-end reads. *BMC Bioinformatics* **15**, 182 (2014).
73. A. Dobin, C. A. Davis, F. Schlesinger, J. Drenkow, C. Zaleski, S. Jha, P. Batut, M. Chaisson, T. R. Gingeras, STAR: Ultrafast universal RNA-seq aligner. *Bioinformatics* **29**, 15–21 (2013).
74. S. Anders, P. T. Pyl, W. Huber, HTSeq—A Python framework to work with high-throughput sequencing data. *Bioinformatics* **31**, 166–169 (2015).
75. M. I. Love, W. Huber, S. Anders, Moderated estimation of fold change and dispersion for RNA-seq data with DESeq2. *Genome Biol.* **15**, 550 (2014).
76. C. E. Grant, T. L. Bailey, W. S. Noble, FIMO: Scanning for occurrences of a given motif. *Bioinformatics* **27**, 1017–1018 (2011).
77. T. L. Bailey, M. Boden, F. A. Buske, M. Frith, C. E. Grant, L. Clementi, J. Ren, W. W. Li, W. S. Noble, MEME SUITE: Tools for motif discovery and searching. *Nucleic Acids Res.* **37**, W202–W208 (2009).
78. W. J. Kent, C. W. Sugnet, T. S. Furey, K. M. Roskin, T. H. Pringle, A. M. Zahler, D. Haussler, The human genome browser at UCSC. *Genome Res.* **12**, 996–1006 (2002).
79. J.-A. Park, J. M. Drazen, D. J. Tschumperlin, The chitinase-like protein YKL-40 is secreted by airway epithelial cells at base line and in response to compressive mechanical stress. *J. Biol. Chem.* **285**, 29817–29825 (2010).
80. M. A. Swartz, D. J. Tschumperlin, R. D. Kamm, J. M. Drazen, Mechanical stress is communicated between different cell types to elicit matrix remodeling. *Proc. Natl. Acad. Sci. U.S.A.* **98**, 6180–6185 (2001).

Acknowledgments: We thank S. Randell at the Marisco Lung Institute, The University of North Carolina at Chapel Hill for providing primary HBECs [National Institutes of Health (NIH) grant number P30DK065988]. **Funding:** This work was funded by the National Cancer Institute (NCI grant number U01CA202123), the National Heart Lung and Blood Institute (NHLBI) grant numbers NHLBI 1R01HL148152, UH3 OD023268, P01HL120839, P01HL132825, T32HL007118, and K25HL133599), the Parker B. Francis Foundation, the Lemann Foundation, the German National Science Foundation (Deutsche Forschungsgemeinschaft), and the American Heart Association (13SDG14320004). This work was conducted with support from Harvard Catalyst, The Harvard Clinical and Translational Science Center (National Center for Advancing Translational Sciences, NIH Award UL1TR002541) and financial contributions from Harvard University and its affiliated academic health care centers. The content is solely the responsibility of the authors and does not necessarily represent the official views of Harvard Catalyst, Harvard University and its affiliated academic health care centers, or the NIH. **Author contributions:** M.D.M., A.K., and E.M. analyzed the data. M.D.M., A.K., K.G., and S.T.W. interpreted the data. M.D.M. and A.K. wrote the manuscript. J.A.M., M.M., C.M., M.J.O., R.C., J.J.F., J.-A.P., and S.T.W. designed the experiment and generated the experimental data. All the authors contributed to the writing of the paper, provided critical feedback, and helped shape the research and the analysis of the problem. **Competing interests:** The authors declare that they have no competing interests. **Data and materials availability:** All data needed to evaluate the conclusions in the paper are present in the paper and/or the Supplementary Materials. Additional data related to this paper may be requested from the authors.

Submitted 5 October 2020

Accepted 7 June 2021

Published 23 July 2021

10.1126/sciadv.abf1088

Citation: M. De Marzio, A. Kılıç, E. Maiorino, J. A. Mitchell, C. Mwase, M. J. O’Sullivan, M. McGill, R. Chase, J. J. Fredberg, J.-A. Park, K. Glass, S. T. Weiss, Genomic signatures of the unjamming transition in compressed human bronchial epithelial cells. *Sci. Adv.* **7**, eabf1088 (2021).